# Thermal rectification of a vanadium dioxide based conductive thermal diode under transient Dirichlet conditions

Cagatay Haratoka, Karl Joulain, Younès Ezzahri

# Thermal rectification of a vanadium dioxide based conductive thermal diode under transient Dirichlet conditions

Cagatay Haratoka*, Karl Joulain, and Younès Ezzahri*

*Institut Pprime, CNRS, Université de Poitiers, ISAE-ENSMA, F-86962 Futuroscope Chasseneuil, France*

**Abstract**

We focus in this work on analysing the behaviour of a thermal diode and consider its operation in the conductive heat transfer regime. The thermal rectification of a thermal diode made of $VO_2$ and $SiO_2$, is investigated in detail by changing different intrinsic and extrinsic parameters under the Dirichlet boundary conditions. The behaviour of the thermal diode is numerically examined according to each parameter individually. We found that the thermal rectification factor can rise to very high values in the first moments of the transient process before reaching steady-state conditions. This feature makes the study of the thermal diode behaviour under transient conditions very promising to pave the way for a better control of practical thermal management systems.

*Keywords:* Thermal rectification, thermal diode, phase change materials (PCM), vanadium dioxide, thermal conductivity, specific heat.

## 1. Introduction

Thermal management is becoming one of the most important engineering endeavours, especially after encountering problems such as global warming, energy crisis and system safety [1]. Thermal management is essential to keep the

*Corresponding authors

*Email addresses:* cagatay.haratoka01@univ-poitiers.fr (Cagatay Haratoka), younes.ezzahri@univ-poitiers.fr (Younès Ezzahri)

temperature within a certain level for various applications for both performance, longevity of operation and safety such as electronic packages [1], photovoltaic panels [2], batteries [3] and thermal storage systems [4]. The thermal diode, which is analogous to the electronic diode, is an attractive and encouraging device to generate thermal rectification for different thermal management applications. It is a two-terminal system that rectifies the heat flux depending on the direction of the temperature gradient between the boundaries of the two terminals. An ideal thermal diode allows heat transfer in one direction according to the difference of temperatures at the terminals, and it blocks it in the opposite direction when the temperatures are exchanged [5–7].

Thermal rectification is a process that occurs as soon as the device thermal properties depend on the temperature so that the heat flux depends on the direction of the temperature gradient [7]. The topic was firstly studied in 1936 by Starr [8]. Starr examined thermal rectification of Copper/Cuprous Oxide interfaces experimentally. Among thermal rectification devices, researches on thermal diodes have dramatically increased in the past decade [1, 5, 6]. There are thermal diodes based on the principles of the three modes of heat transfer: conduction, convection and radiation [5–7]. Graphene based heterostructures, in which thermal rectification occurs due to asymmetrical phonon propagation at the material interface, are widely under investigation in the literature as an example for the principle of conduction [9–13]. In addition, there are also studies on functionally graded materials to obtain thermal rectification [14–18]. These are the materials whose composition along an axis changes and causes thermal rectification due to different material properties along the axis. Although functionally graded materials have a potential for mass production due to being constructed by one material, they need more experimental studies [5]. Moreover, thermal rectification can also be obtained using superconductor materials, but there are limited studies about thermal diodes based on superconductors [5].

Phase change materials (PCM) are another alternative to generate thermal rectification. It is worth mentioning that PCM have different contexts in different communities. They include solid-liquid transition as well as crystal structure transformation (crystalline-amorphous transition and dielectric-metallic transition). Consequently, they manifest different thermal, electrical and optical properties according to their critical temperature of transition [19]. Therefore, thermal diodes based on PCM constitute a beneficial solution for thermal management due to their altering characteristics. Among PCM, vanadium dioxide ($VO_2$), which is one of the most popular PCM, has recently drawn great attention thanks to the closeness of its critical transition temperature to room temperature. It is an ideal candidate to manipulate conductive heat flux and in which thermal rectification can occur. $VO_2$ shows a metal-insulator transition (MIT) around a critical temperature, which is $T_o$ = 341 K [20]. The crystalline structure of $VO_2$ shows monoclinic and tetragonal-rutile crystalline structures below and above $T_o$, respectively [21]. The metallic phase results in a high thermal conductivity above $T_o$, whereas the dielectric phase results in a low thermal conductivity below it [22].

In the literature, available studies mostly focused on exploring conductive thermal rectification under steady-state conditions. Yang et al. [23] modelled a thermal diode that consists of two materials with linear temperature-dependent thermal conductivities based on Fourier's law of heat conduction and carried out a study to optimize the thermal rectification. They obtained a maximum rectification ratio of 0.5 [23]. However, reaching this high rectification ratio is difficult and costly, because there is a need for a high temperature difference larger than 100 K to obtain it [23]. As a practical advantage of PCM, this drawback can be overcome thanks to their thermal conductivity alteration to some extent. Thus, there are detailed investigations to use $VO_2$ in thermal diodes as a single PCM or in combination with another PCM. [24–28]. Ordonez-Miranda et al. [27] examined a thermal diode with a single PCM, ($VO_2$ or nitinol) under steady-state conditions. They reached 19.7% of thermal rectification and concluded that a higher thermal conductivity contrast, smaller thermal hysteresis and faster phase transition can generate higher thermal rectification. Moreover, Kasali et al. [24] theoretically investigated the thermal diode that was made by two PCM as the combination of $VO_2$ and Polyethylene. In their study, they reached a thermal rectification of 60%. Later, they analysed the influence of the diode geometry. They obtained a thermal rectification of 63.5% and 63.2% for spherical and cylindrical thermal diodes, respectively, that were made by $VO_2$ and Polyethylene. These values of thermal rectification, which are very close, are higher than the one obtained in the plane geometry [28].

Nevertheless, not much effort has been devoted to the study of conductive thermal rectification under transient conditions. The latter needs to be well understood to be able to utilize thermal components practically and efficiently. Herrera et al. [29] published the first study related to thermal diodes under transient conditions. They calculated the thermal rectification of thermal diodes whose thermal conductivity varies linearly with temperature by applying finite difference method. Also, they introduced time-dependent thermal rectification factor and observed a higher rectification factor under transient conditions [29]. Klinar et al. [30] carried out a numerical study to investigate the influence of a thermal diode in a magnetocaloric refrigeration device. They analysed various temperature dependent thermal conductivity profiles and found out that the thermal rectification reaches higher values under transient conditions than steady-state conditions.

There are many studies that examine the thermal rectification of thermal diodes in steady-state conditions and the interest for transient analysis is increasing. However, we have not encountered any prior work that studied thermal diodes while considering properties of $VO_2$ in full aspects under transient conditions. Therefore, the objective as well as the novelty of this study is to investigate a thermal diode based on a single PCM, under transient conditions. The thermal diode is made of $VO_2$ and $SiO_2$ and we consider the Dirichlet boundary conditions to be applied. The thermal conductivity and the specific heat of $VO_2$ depend strongly on temperature, mainly in the vicinity of the critical transition temperature [20]. On the other hand, the changes of the thermal conductivity and the specific heat of $SiO_2$ with temperature are negligible. The thermal rectification of the thermal diode is investigated in detail by changing different intrinsic and extrinsic parameters.

## 2. Theoretical modelling

We consider a thermal diode in a plane geometry that is made of a PCM and non-PCM in this study as stated before. We assume this thermal diode to be placed between two thermal baths in a vacuum chamber so that we can neglect any heat exchange due to convection. We also assume heat exchange due to radiation to be negligible and consider conduction to be the only heat transfer mode between the two thermal baths. Therefore, there is a conductive heat exchange between the two thermal baths due to their temperature difference $T_h - T_c$, as illustrated in Fig.1. The heat flux flows from the PCM to the non-PCM in the forward configuration. Conversely, it flows in the opposite direction in the backward configuration. Heat fluxes in forward and backward configurations are driven by the thermal conductivities of the PCM and non-PCM. The total length of the model is $2l$ and both materials have equal lengths, which mean half of the total length, as shown in Fig.1.

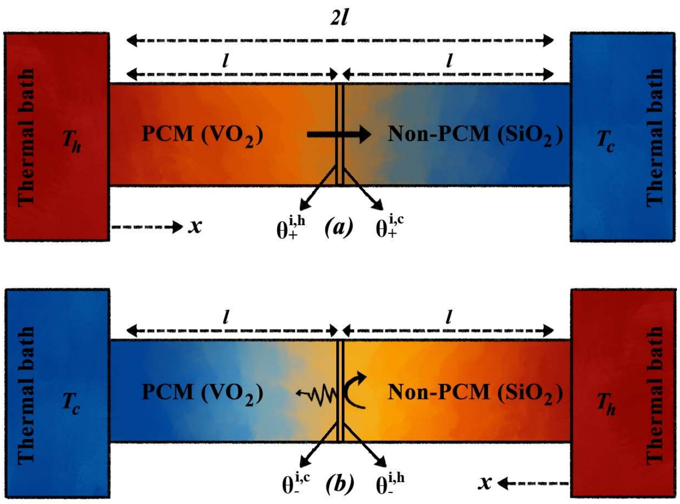


Figure 1: Schematic representation of the studied thermal diode in the forward and backward configurations.

### *2.1. Nondimensionalization of the transient process*

The nonlinear heat diffusion equation for $VO_2$ is given by:

$$\rho_v c_p(T)\frac{\partial T}{\partial t} = \frac{\partial}{\partial x}\left[k(T)\frac{\partial T}{\partial x}\right] \tag{1}$$

The thermal conductivity, $k(T)$, and specific heat capacity, $c_p(T)$, of $VO_2$ vary with temperature. The thermal conductivity of $VO_2$ can be described using the following equation [27].

$$k(T) = k_d + \frac{k_m - k_d}{1+e^{-\beta(T-T_O)}} \tag{2}$$

where $k_d$ and $k_m$ represent the thermal conductivity of $VO_2$ in the dielectric and metallic phases, respectively. $T_o$ is the phase critical transition temperature and $\beta$ is the phase transition slope. The values of these parameters are as follows: 3.6 $W.m^{-1}.K^{-1}$ for $k_d$, 6 $W.m^{-1}.K^{-1}$ for $k_m$ and 1.6 $K^{-1}$ for $\beta$. The values of $k_d$ and $k_m$ were measured experimentally by Oh et al. [22], while the value of $\beta$ corresponds to the best fit of the experimental data using Eq.2 [27]. In addition, $T_0$ takes the values $T_{oh}$ = 342.9 K and $T_{oc}$ = 334.9 K during the heating and cooling processes respectively due to 8 K hysteresis effect of $VO_2$ between these processes [27]. Therefore, $T_{oh}$ and $T_{oc}$ represent the transition temperatures of the heating and cooling processes, respectively.

As reported in Ref [31], the expression of the specific heat capacity of $VO_2$ is given by:

$$c_p(T) = c_d(T) + T\frac{\delta^2}{\rho_v \gamma} + L_n \frac{\partial f}{\partial T} \tag{3}$$

where $c_d$, $\rho_v$, $\delta$, $\gamma$ and $L_n$ represent the specific heat capacity predicted by Debye model, density of $VO_2$, coefficient of thermal expansion, isothermal compressibility and latent heat, respectively. Since the variation of $c_d$ within the range of the considered boundary conditions (BC) is negligible, we assume it to be constant and we take the average of the values of $c_d$ at the BC temperatures as 0.704 kJ.kg$^{-1}$.K$^{-1}$. Moreover, $\rho_v$ of $VO_2$ changes according to its crystalline structure. However, for simplicity sake throughout the study, we assume $\rho_v$ to be also constant and we take the average of the values of the dielectric monoclinic and metallic tetragonal-rutile crystalline structures as 4612 kg.m$^{-3}$. $L_n$ equals 51.45 kJ.kg$^{-1}$ for the heating process of $VO_2$ [32] and we assume the same value for the cooling process. As explained in the study of Ordonez-Miranda et al. [31], the second term in the right side of Eq.3 can be neglected, because the values of this term are much smaller than the values of $c_d$ within the phase transition temperatures interval. Thus, its contribution is neglected throughout the study. The temperature behaviours of the thermal conductivity and specific heat capacity of $VO_2$ are reported in Figs.2(a) and 2(b), respectively.

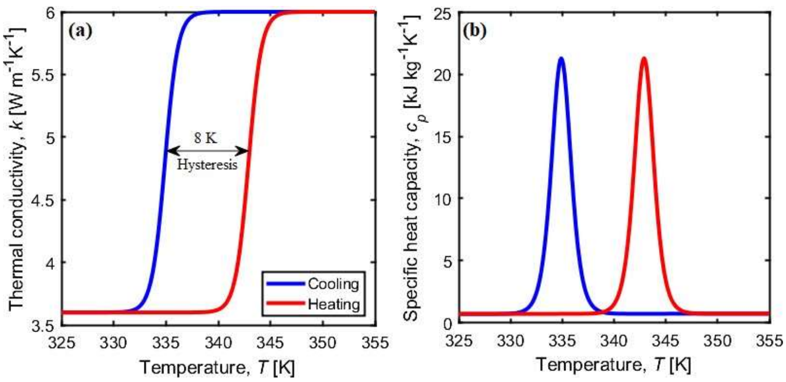


Figure 2: Computed behaviours of the (a) thermal conductivity and (b) specific heat capacity of $VO_2$ as functions of temperature.

Eq.1 can be nondimensionalized easily as

$$\frac{\bar{\alpha}}{\alpha_d}\left[1+\frac{L_n}{c_d \Delta T_o}\frac{\partial f}{\partial \theta}\right]\frac{\partial \theta}{\partial t^*} = \frac{\partial}{\partial x^*}\left\{\left[1+(k_r-1)f(\theta)\right]\frac{\partial \theta}{\partial x^*}\right\} \qquad (4)$$

where the dimensionless temperature is defined by $\theta = (T - T_o)/\Delta T_o$, the dimensionless length by $x^* = x/l$ and the dimensionless time by $t^* = \bar{\alpha}t/l^2$. $\Delta T_o$ is the difference between the transition temperatures of heating and cooling processes: $\Delta T_o = T_{oh} - T_{oc}$. $\bar{\alpha}$ is the average thermal diffusivity between the one of the dielectric structure of $VO_2$ and $SiO_2$, which is $\bar{\alpha} = (\alpha_d + \alpha_s)/2$. $\alpha_d$ and $\alpha_s$ represent the thermal diffusivity of the dielectric structure of $VO_2$ and $SiO_2$, respectively. They are given by $\alpha_d = k_d/(\rho_v c_d)$ and $\alpha_s = k_s/(\rho_s c_s)$. $\rho_v$ and $\rho_s$ are the densities of $VO_2$ and $SiO_2$ in order. The thermal conductivity, $k_s$, specific heat capacity, $c_s$, and density, $\rho_s$, of $SiO_2$ are 1.5 W.m$^{-1}$.K$^{-1}$, 0.73 kJ.kg$^{-1}$.K$^{-1}$ and 2650 kg.m$^{-3}$, respectively. $k_r$=$k_m/k_d$ and $f(\theta)$ is expressed as $f(\theta) = \left[1 + e^{-\beta \Delta T_o \theta}\right]^{-1}$.

Moreover, the heat diffusion equation in $SiO_2$, whose changes of the thermal conductivity and the specific heat capacity with temperature are negligible, can be nondimensionalized straightforwardly as

$$\frac{\bar{\alpha}}{\alpha_s}\frac{\partial \theta}{\partial t^*} = \frac{\partial^2 \theta}{\partial {x^*}^2} \tag{5}$$

Eq.(4-5) are numerically solved by using implicit finite difference method and discretized in time and space for many nodes. Finally, the normalized heat flux density (ratio of the heat flux density to the quantity $\Delta T_o/l$) can be evaluated by using Eq.6 and Eq.7 for forward and backward configurations.

$$\Phi_+^* = -k_s \frac{\partial \theta}{\partial x^*} \tag{6}$$

$$\Phi_-^* = -k_d[1 + (k_r - 1)f(\theta)]\frac{\partial \theta}{\partial x^*} \tag{7}$$

where + and - signs represent forward and backward fluxes, respectively. Even though the quantities expressed in Eq.6 and Eq.7 have the dimension of a thermal conductivity, we will refer to them as nondimensional heat flux densities henceforth in this paper.

The interface thermal resistance describing the temperature discontinuity at the interface between the two slabs of $VO_2$ and $SiO_2$ is also modelled according to the study of Yuan et al. [33]. The authors developed two one-dimensional models, that represent the interface thermal resistance with a virtual layer or an artificial layer, to analyse the heat transfer in multi layered materials including the interface thermal resistance. In our study, we create an artificial layer with a width of $\Delta x$ between the two materials. Half of the length of the artificial layer is overlaid in the left material and the other half is in the right material, which are $VO_2$ and $SiO_2$, respectively. The artificial layer has the modified thermal properties according to the features of $VO_2$ and $SiO_2$ to represent their effects at the interface of these two materials as explained in the study of Yuan et al. [33]. We define an effective thermal conductivity, $k_e$, that takes into account the effects of the thermal conductivities of the artificial layer, $VO_2$ and $SiO_2$ as [33]

$$\frac{1}{k_e} = \frac{1}{k_i} + \frac{1}{2k_v} + \frac{1}{2k_s} \tag{8}$$

$k_i$ is the thermal conductivity of the artificial layer and can be defined as $k_i = \Delta x/r$, where $r$ is the interface thermal resistance. Details of this model are explained in the reference [33].

### *2.2. Nondimensionalization of the steady-state process*

The heat conduction equation is solved under steady-state conditions semi-analytically in order to validate the results of the steady-state regime that were numerically obtained during the transient regime analysis. The following Eqs.(9-12) are obtained after Eq.1 was nondimensionalized under steady-state conditions:

$$\xi\left(\theta_{+}^{i,h}\right) + \left[k_r + \frac{k_s}{k_d(1+\eta k_s)}\right]\theta_{+}^{i,h} = \xi\left(\theta^{h}\right) + k_r\theta_h + \frac{k_s\theta_c}{k_d\left(1+\eta_{k_s}\right)} \quad (9)$$

$$\xi\left(\theta_{-}^{i,c}\right) + \left[k_r + \frac{k_s}{k_d(1+\eta k_s)}\right]\theta_{-}^{i,c} = \xi\left(\theta^{c}\right) + k_r\theta_c + \frac{k_s\theta_h}{k_d\left(1+\eta_{k_s}\right)} \quad (10)$$

where $\xi(\theta) = \left[(k_r - 1)ln\left(1 + e^{-\beta\Delta T_o\theta}\right)\right] / [\beta\Delta T_o]$. $\theta_{+}^{i,h}$ and $\theta_{-}^{i,c}$ are the nondimensional temperatures of the hot and cold sides at the interface of two materials in the forward and backward configurations, respectively, as illustrated in Fig.1 above. $\theta_h$ and $\theta_c$ are the hot and cold nondimensional BC temperatures, respectively. In addition, $\eta$ is defined by $r/l$.

Eqs. 9 and 10 allow determining $\theta_{+}^{i,h}$ and $\theta_{-}^{i,c}$ as a function of $\theta_h$, $\theta_c$ and the rest of the system parameters. Once $\theta_{+}^{i,h}$ and $\theta_{-}^{i,c}$ are determined, we can obtain straightforwardly $\theta_{+}^{i,c}$ and $\theta_{-}^{i,h}$ via the following Eqs. 11 and 12:

$$\theta_{+}^{i,c} = \frac{\theta_{+}^{i,h}/\eta + k_s\theta_c}{1/\eta + k_s} \quad (11)$$

$$\theta_{-}^{i,h} = \frac{\theta_{-}^{i,c}/\eta + k_s\theta_h}{1/\eta + k_s} \quad (12)$$

### *2.3. Thermal rectification analysis*

In the absence of an internal heat source, the heat flux remains constant throughout the system under steady-state conditions. Therefore, thermal rectification can be calculated using the ratio of the difference between forward and backward heat fluxes to the maximum heat flux between the two configurations. However, this is not valid for transient conditions as emphasized by Herrera et al. [29], because heat flux can vary throughout the system under these conditions. Thus, we analysed the thermal rectification on the basis of the heat flux density at the cold end by considering the fact that heat spontaneously moves from the hot side to the cold side according to the second law of thermodynamics. Consequently, we define the thermal rectification as

$$R(t^*) = \frac{|\Phi_+^* - \Phi_-^*|}{max(\Phi_+^*, \Phi_-^*)} \tag{13}$$

The thermal rectification is evaluated using three different metrics as proposed by Herrera et al. [29]: (a) The first metric is $R_{max}$ which represents the maximum thermal rectification factor, (b) the second metric is $R_{ss}$ which is the thermal rectification factor at steady-state conditions, and (c) the third metric is the time-integrated thermal rectification factor, $\tilde{R}$, which allows a better quantification of the capacitive effects,

$$\tilde{R} = \int_{t_m^*}^{t_{ss}^*} R(t^*) dt^* \tag{14}$$

where $t_{ss}^*$ and $t_m^*$ represent the times for which $R_{ss}$ and the first peak in the thermal rectification profile are reached, respectively. It is also worth mentioning that the first peak in the thermal rectification profile as a function of time coincides very often with $R_{max}$. As a general rule, we considered $t^*_{ss}$ to be the time at which the full numerical solution of the thermal rectification in the transient regime analysis equals 99% of the semi-analytical solution obtained under steady-state conditions. In the case of the steady-state analysis, we can easily show that the thermal rectification factor is given by:

$$R_{ss} = \frac{\left|(\theta_h + \theta_c) - \left(\theta_+^{i,c} + \theta_-^{i,h}\right)\right|}{max\left\{\left(\theta_+^{i,c} - \theta_c\right), \left(\theta_h - \theta_-^{i,h}\right)\right\}} \tag{15}$$

### 3. Results and discussion

In our analysis of the time dependent thermal rectification behaviour of the suggested $VO_2$ based conductive thermal diode under the transient Dirichlet conditions, we explore the consequences of two initial conditions: $T(t = 0) = T_c$ leading to a heating process of the full system and $T(t = 0) = T_h$ which leads to a cooling process. We investigate the impact of varying six different parameters; BC change, $\beta$, $L_n$, $k_r$, $\Delta T_o$ and r. During the study, only one parameter is changed in each analysis and the rest is kept unchanged. We firstly consider four different BC cases according to the real features of $VO_2$ and $SiO_2$. Then, we deeply analyse the remaining parameters with five different cases individually by considering the BC to be $T_h = 354$ K and $T_c = 324$ K. The cases for each parameter are shown in Table 1.

In the first analysis of the four different BC, we consider $T_h$ and $T_c$ for the heating and cooling conditions, separately, according to the real characteristic values of $VO_2$ and $SiO_2$. We fix these values with respect to $T_o$, which takes the value of 342.9 K for $T_{oh}$ and the value of 334.9 K for $T_{oc}$, as stated before. In order to check the effect of the phase transition of $VO_2$ on the thermal rectification in detail, we specify the values of temperatures for the BC in various intervals surrounding the phase transition area of $VO_2$, which was previously shown in Fig.2. We report in Figs.3, the computed time behaviours of the nondimensional heat flux density at the cold boundary [Figs.3(a) and 3(c)] in the forward and backward configurations and the thermal rectification factor [Figs.3(b) and 3(d)] for both the heating [Figs.3(a) and 3(b)] and cooling [Figs.3(c) and 3(d)] processes of the full thermal diode. As our modelling is based on Fourier's law, we only account for times beyond the diffusion time in order to avoid the drawback of the parabolic nature of the heat equation. The diffusion time corresponds to the time required for the temperature front to diffuse from the hot boundary to the cold one and can roughly be estimated as $l^2/\overline{\alpha}$. The general trend is the same for the different values of BC in each process and each configuration. In the heating process, the nondimensional heat flux density increases with time to saturate at the steady-state values for both forward and backward configurations, while there is a decreasing behaviour in the cooling process. As expected the value of nondimensional heat flux density increases by increasing the tem-

Table 1: Investigated parameters and cases.

| | | | | | |
|---|---|---|---|---|---|
| | | | Case 1 - BC | | |
| | (i) | (ii) | (iii) | (iv) | |
| | | | Heating analysis | | |
| $T_h$ [K] | 348 | 353 | 358 | 363 | |
| $T_c$ [K] | 338 | 333 | 328 | 323 | |
| | | | Cooling analysis | | |
| $T_h$ [K] | 340 | 345 | 350 | 355 | |
| $T_c$ [K] | 330 | 325 | 320 | 315 | |
| | | | Case 2 - $\beta$ | | |
| | (i) | (ii) | (iii) | (iv) | (v) |
| $\beta$ [$K^{-1}$] | 0.5 | 1 | 1.6 | 3 | 5 |
| | | | Case 3 - $L_n$ | | |
| | (i) | (ii) | (iii) | (iv) | (v) |
| $L_n$ [kJ.kg$^{-1}$] | 66.89 (+30%) | 59.17 (+15%) | 51.45 | 43.73 (-15%) | 36.02 (-30%) |
| | | | Case 4 - $k_r$ | | |
| | (i) | (ii) | (iii) | (iv) | (v) |
| $k_r$ | 1.2 | 1.5 | 1.667 | 3 | 5 |
| | | | Case 5 - $\Delta T_o$ | | |
| | (i) | (ii) | (iii) | (iv) | (v) |
| $\Delta T_o$ [K] | 2 | 5 | 8 | 13 | 17 |
| | | | Heating analysis | | |
| $T_{oh}$ [K] | 336.9 | 339.9 | 342.9 | 347.9 | 351.9 |
| | | | Cooling analysis | | |
| $T_{oc}$ [K] | 340.9 | 337.9 | 334.9 | 329.9 | 325.9 |
| | | | Case 6 - $r$ | | |
| | (i) | (ii) | (iii) | (iv) | (v) |
| r [m$^2$.K.W$^{-1}$] | $10^{-1}$ | $10^{-2}$ | $10^{-3}$ | $10^{-4}$ | $10^{-5}$ |

perature difference between the two boundaries. It is interesting to note that the saturation dynamics of the nondimensional heat flux density in the heating and cooling processes switches between the forward and backward configuration in each process by changing $\Delta T = T_h - T_c$. Indeed, while the nondimensional heat flux density seems to saturate faster (slower) by increasing $\Delta T$ for the forward (backward) configuration in the heating process, the opposite occurs in the cooling process. The behaviour of the thermal rectification factor $R$ shows interesting nonlinear features, which are consequences of the behaviour of the nondimensional heat flux densities in the forward and backward configurations for each process. In both the heating and cooling processes, $R$ manifests a maximum $R_{max}$, goes to zero, then increases again to reach the steady-state

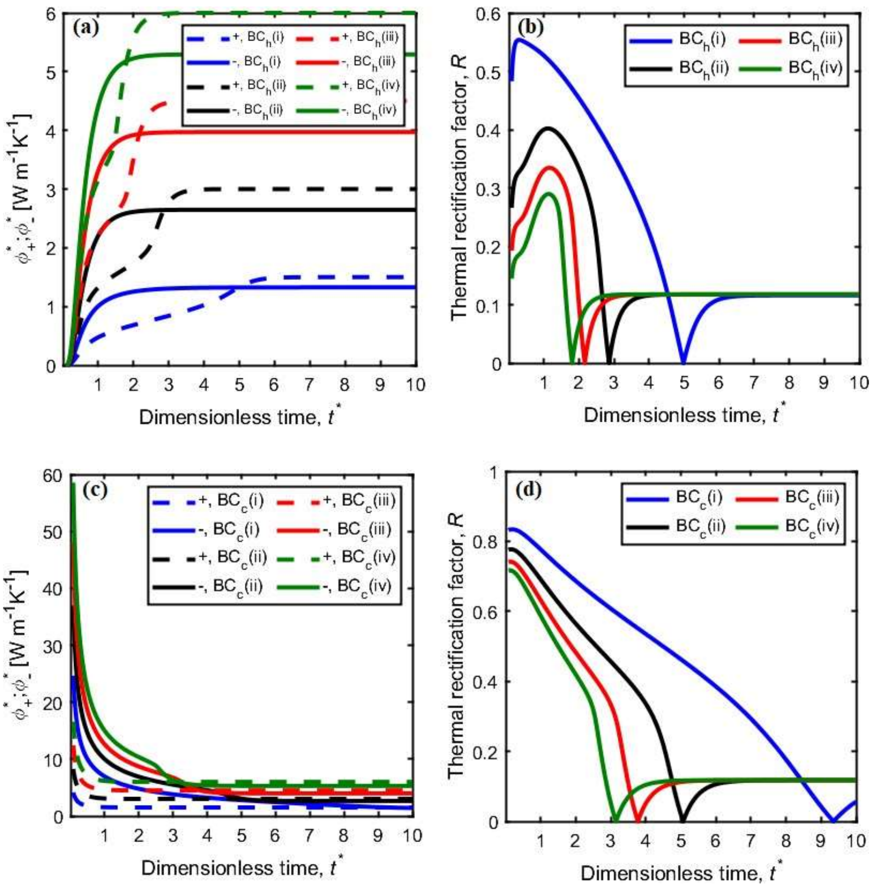


Figure 3: Computed time behaviours of the nondimensional heat flux density and thermal rectification factor in the heating [(a) and (b)] and cooling [(c) and (d)] processes, respectively, for different values of BCs.

value. $R_{max}$ has a higher amplitude and occurs in early times in the cooling process in comparison to the heating process. This difference between the two processes is a direct result of the combined initial condition effect and the side nature (cold) of the thermal diode at which thermal rectification is considered and analysed. The time at which $R$ vanishes in the cooling process is almost double the one for the heating process. An indication that the dynamics of the thermal rectification lasts longer in the cooling process in comparison to the heating process. The steady-state regime values of $R$ are therefore attained in longer periods in the cooling process. We also notice that the time at which the steady-state regime values are reached increases by decreasing $\Delta T$. When the intervals of BCs are getting shorter and the values of their temperatures approach the critical temperature of the phase transition process of $VO_2$, higher $R_{max}$ and $\tilde{R}$ are obtained. In addition to this, the thermal rectification factor $R$ in the steady-state regime is almost independent with respect to the values of $\Delta T$.

As expressed by Eqs.2 and 3, the thermal conductivity $k$ and specific heat capacity $c_p$ of $VO_2$, depend strongly on the parameter $\beta$ which describes the phase transition slope in the temperature behaviour of $k$. The variation of this parameter affects considerably the temperature profile of these two properties. Indeed, by decreasing $\beta$, the jump from the dielectric value $k_d$ to the metallic value $k_m$ becomes less steep and the amplitude of $c_p$ decreases. On the other hand, sharper transition behaviour occurs in $k$ and higher $c_p$ are observed when $\beta$ increases. By changing $\beta$, the main features in the time profile of $\Phi_+^*$, $\Phi_-^*$ and $R$, are almost similar to the ones shown in Figs.3. Although, the variation of $\beta$ seems to have almost no effect on the behaviour of $\Phi_+^*$ and $\Phi_-^*$ , the impact is more pronounced in the behaviour of $R$. Interestingly also, it is the fact that varying $\beta$ affects more $R_{max}$ in the heating process and the time of $R$ vanishing in the cooling process, in comparison to the opposite process, respectively. $R_{max}$ decreases by increasing $\beta$. The effect of $\beta$ becomes less pronounced in the steady-state regime. Furthermore, we notice an almost continuous decrease in $\tilde{R}$ as $\beta$ increases for the heating process, but we do not see this trend in the cooling process.

The specific heat capacity $c_p$ has a direct effect on heat transfer under transient conditions. In the case of $VO_2$ and as we discussed it above, the latent heat $L_n$ plays a key role in the behaviour of $c_p$. We report in Figs.4(a) and 4(b), the computed time behaviours of the thermal rectification factor $R$ in the heating and cooling processes, respectively, for different values of $L_n$. The main features in the time profile of $R$, remain similar to the ones shown in Figs.3(b) and 3(d). While varying $L_n$ affects more $R_{max}$ in the heating process than in the cooling process similarly to the effect of $\beta$, it influences the time at which $R$ vanishes in both processes. Additionally, $R_{max}$ and $\tilde{R}$ decrease by decreasing $L_n$ for both processes. In the steady-state regime, the effect of $L_n$ disappears and all the curves collapse on each other as expected. $c_p$ has no impact on the heat transfer under steady-state conditions.

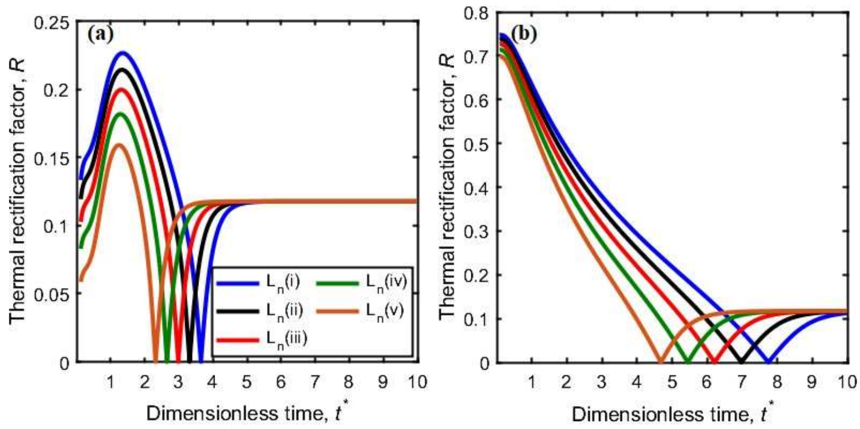


Figure 4: Computed time behaviours of the thermal rectification factor in the heating (a) and cooling (b) processes, for different values of the parameter $L_n$.

The fourth parameter we considered in our study is the ratio of the thermal conductivity of the metallic and dielectric phases of $VO_2$, $k_r$. We show the computed time behaviours of the thermal rectification factor $R$ in the heating and cooling processes, in Figs.5(a) and 5(b), respectively, for different values of $k_r$. While in the cooling process, the features remain similar to the case of varying $\Delta T = T_h - T_c$, $\beta$ and $L_n$, the time profiles of $R$ in the heating process manifest interesting additional nonlinear features depending on the value of $k_r$. When $k_r$ increases, the values of $R_{max}$ and $\tilde{R}$ decrease until the third case, which is the result according to the real characteristic value of $VO_2$. Above the third value of $k_r$, the behaviour of $R$ as a function of the nondimensional time changes drastically in the early moment of the transient process. Three and two peaks appear in the fourth and fifth cases, respectively, instead of just one as in the three first cases. Besides, the third peak, which is barely seen, occurs just before the value of $R_{ss}$ in the fourth case. Thus, the value of $R_{ss}$ is extremely close to the value of the third peak in this case while the second peak in the fifth case gets even higher than the previous cases. Moreover, there is no systematic trend in the intersection of the nondimensional heat flux densities of the forward and backward configurations causing zero thermal rectification, it may appear more

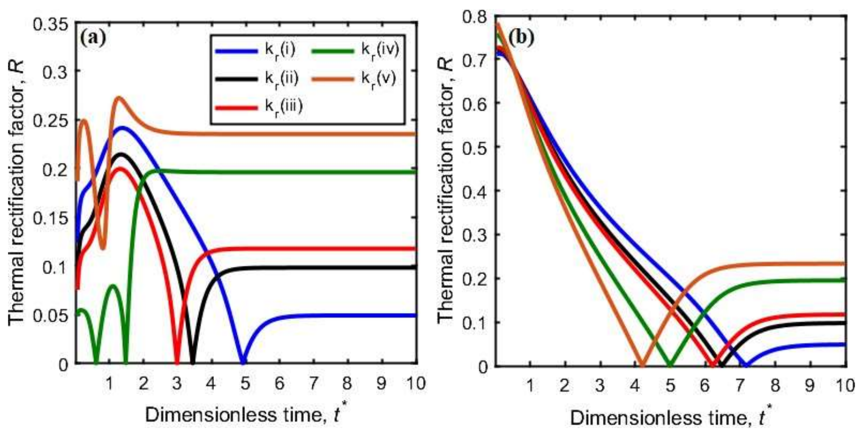


Figure 5: Computed time behaviours of the thermal rectification factor in the heating (a) and cooling (b) processes, for different values of the parameter $k_r$.

than once as in the fourth case or not at all as in the fifth case. Interestingly, by increasing $k_r$, the value of $R_{ss}$ increases and it is reached faster in both the heating and cooling processes. Generally, varying $k_r$ impacts strongly the entire time profile of $R$ spanning from the early transient regime to the steady-state regime.

There is a $\Delta T_o = T_{oh} - T_{oc} = 8$ K hysteresis effect of $VO_2$ between the phase transition temperatures for heating and cooling processes as stated before. The values of the phase transition temperatures; $T_{oh}$, $T_{oc}$ and the hysteresis effect have a direct influence on the thermal rectification of the conductive thermal diode as a consequence of the dependence of the thermal conductivity $k$ and specific heat capacity $c_p$ on these parameters as expressed by Eqs.2 and 3. We examined the influence on the thermal rectification factor by considering different values of $\Delta T_o$. These values are obtained by varying $T_{oh}$ and $T_{oc}$, for the heating and cooling processes, respectively, while keeping the other temperature fixed as shown in Table 1 above. When $T_{oh}$ and $T_{oc}$ get closer to the BC, in other words, when $\Delta T_o$ increases, lower $R$ and $R_{max}$ are observed for both the heating and cooling processes of the thermal diode as reported in Figs.6(a) and 6(b), respectively. However, we can not identify any systematic trend for $\tilde{R}$. Indeed, it is interesting to note that in the first four cases of the cooling process, $\tilde{R}$ increases by increasing $\Delta T_o$. Nevertheless, the fifth case shows a sudden decrease. This sudden decrease can also be seen in the fifth case of the heating process. Besides, in the fourth and fifth cases, the amplitude of the first peak in the thermal rectification time profile in the heating process, is lower than the value at the steady-state regime. A behaviour that we encountered also while varying the ratio $k_r$ as shown in Fig.5(a). Moreover, $R_{ss}$ decreases by increasing $\Delta T_o$ for both heating and cooling processes.

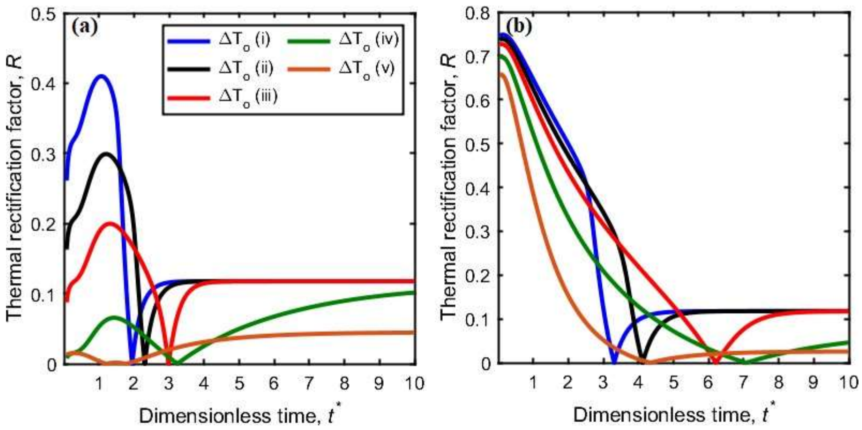


Figure 6: Computed time behaviours of the thermal rectification factor in the heating (a) and cooling (b) processes, for different values of the parameter $\Delta T_o$.

The analysis until this point was carried out by assuming there is no interface thermal resistance between the two slabs of $VO_2$ and $SiO_2$ composing the conductive thermal diode. This constitutes the sixth and last parameter we considered in our parametric study and it is modelled by using the artificial layer approach of Yuan et al. [33] as mentioned in the theory section above. The general trend is similar for the different values of $r$ for heating and cooling processes as reported in Figs.7(a) and 7(b), respectively. Although this effect is not obvious in the cooling process, we get higher $R_{max}$ and lower $R_{ss}$ in the heating process when the value of $r$ increases. Furthermore, especially in the cooling process, $R$ tends to saturate at its steady-state value faster by increasing $r$. Nevertheless, this effect seems to be almost insignificant except between the first two cases. Similarly, it is only between these two cases, where the time-integrated thermal rectification factor $\tilde{R}$ shows a dependence on $r$ in the cooling process. For the rest of the cases, $\tilde{R}$ remains almost constant as for $R_{max}$ and $R_{ss}$. We summarize all the calculated values of $R_{max}$, $R_{ss}$ and $\tilde{R}$ for the different cases of each of the six parameters investigated in this study in Table 2 below.

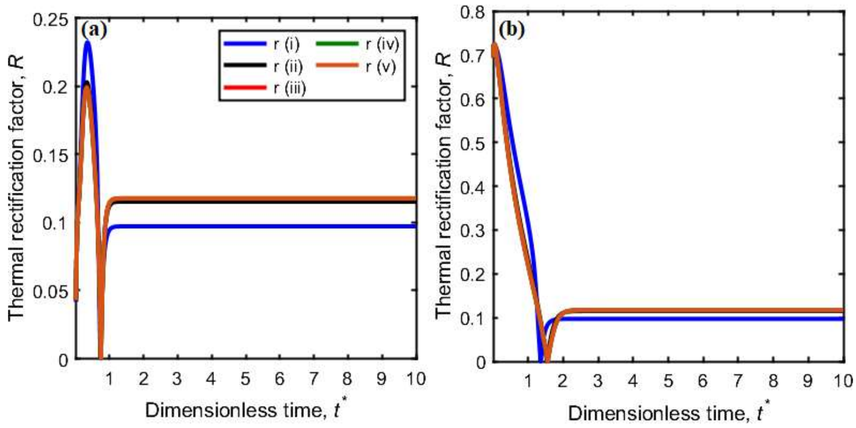


Figure 7: Computed time behaviours of the thermal rectification factor in the heating (a) and cooling (b) processes, for different values of the parameter $r$.

The time dynamics of the thermal rectification has shown to be sensitive to each of the six parameters we considered in this study. It manifests a very pronounced non linear behaviour. The degree of influence is not the same for the different parameters, but they all impact the whole time profile of the thermal rectification, ranging from the early transient regime to the steady-state regime. $R_{max}$, $R_{ss}$ and $\tilde{R}$ all change by varying each of the parameters. $\tilde{R}$ which quantifies the capacitive effect of the conductive thermal diode, gives a central information about the duration and magnitude of the thermal rectification dynamics span.

Table 2: The calculated values for the maximum thermal rectification factor, thermal rectification factor at steady-state conditions and time-integrated thermal rectification factor for all investigated cases.

| | Heating analysis | | | | | Cooling analysis | | | | |
|---|---|---|---|---|---|---|---|---|---|---|
| | Case 1 - BC | | | | | | | | | |
| | (i) | (ii) | (iii) | (iv) | | (i) | (ii) | (iii) | (iv) | |
| $R_{max}$ | 0.55 | 0.40 | 0.33 | 0.29 | | 0.83 | 0.78 | 0.74 | 0.72 | |
| $R_{ss}$ | 0.11 | 0.12 | 0.12 | 0.12 | | 0.11 | 0.12 | 0.12 | 0.12 | |
| $\tilde{R}$ | 1.84 | 0.86 | 0.35 | 0.23 | | 4.58 | 2.54 | 1.88 | 1.54 | |
| | Case 2 - $\beta$ | | | | | | | | | |
| | (i) | (ii) | (iii) | (iv) | (v) | (i) | (ii) | (iii) | (iv) | (v) |
| $R_{max}$ | 0.24 | 0.21 | 0.20 | 0.19 | 0.18 | 0.73 | 0.73 | 0.73 | 0.73 | 0.73 |
| $R_{ss}$ | 0.11 | 0.12 | 0.12 | 0.12 | 0.12 | 0.11 | 0.11 | 0.12 | 0.12 | 0.12 |
| $\tilde{R}$ | 0.48 | 0.37 | 0.35 | 0.34 | 0.34 | 2.19 | 2.28 | 2.25 | 2.25 | 2.29 |
| | Case 3 - $L_n$ | | | | | | | | | |
| | (i) | (ii) | (iii) | (iv) | (v) | (i) | (ii) | (iii) | (iv) | (v) |
| $R_{max}$ | 0.23 | 0.21 | 0.20 | 0.18 | 0.16 | 0.75 | 0.74 | 0.73 | 0.71 | 0.70 |
| $R_{ss}$ | 0.12 | 0.12 | 0.12 | 0.12 | 0.12 | 0.12 | 0.12 | 0.12 | 0.12 | 0.12 |
| $\tilde{R}$ | 0.47 | 0.41 | 0.35 | 0.29 | 0.24 | 2.78 | 2.51 | 2.25 | 1.98 | 1.71 |
| | Case 4 - $k_r$ | | | | | | | | | |
| | (i) | (ii) | (iii) | (iv) | (v) | (i) | (ii) | (iii) | (iv) | (v) |
| $R_{max}$ | 0.24 | 0.21 | 0.20 | 0.05 | 0.25 | 0.71 | 0.72 | 0.73 | 0.75 | 0.78 |
| $R_{ss}$ | 0.05 | 0.10 | 0.12 | 0.20 | 0.24 | 0.05 | 0.10 | 0.12 | 0.19 | 0.23 |
| $\tilde{R}$ | 0.59 | 0.41 | 0.35 | 0.33 | 0.63 | 2.41 | 2.29 | 2.24 | 2.09 | 1.99 |
| | Case 5 - $\Delta T_o$ | | | | | | | | | |
| | (i) | (ii) | (iii) | (iv) | (v) | (i) | (ii) | (iii) | (iv) | (v) |
| $R_{max}$ | 0.41 | 0.30 | 0.20 | 0.07 | 0.02 | 0.75 | 0.74 | 0.73 | 0.70 | 0.66 |
| $R_{ss}$ | 0.12 | 0.12 | 0.12 | 0.11 | 0.04 | 0.12 | 0.12 | 0.12 | 0.08 | 0.03 |
| $\tilde{R}$ | 0.35 | 0.36 | 0.35 | 1.11 | 0.31 | 1.74 | 1.96 | 2.25 | 2.57 | 1.00 |
| | Case 6 - $r$ | | | | | | | | | |
| | (i) | (ii) | (iii) | (iv) | (v) | (i) | (ii) | (iii) | (iv) | (v) |
| $R_{max}$ | 0.23 | 0.20 | 0.20 | 0.20 | 0.20 | 0.72 | 0.72 | 0.72 | 0.72 | 0.72 |
| $R_{ss}$ | 0.10 | 0.11 | 0.12 | 0.12 | 0.12 | 0.09 | 0.11 | 0.12 | 0.12 | 0.12 |
| $\tilde{R}$ | 0.09 | 0.09 | 0.09 | 0.09 | 0.09 | 0.59 | 0.56 | 0.56 | 0.56 | 0.56 |

## 4. Conclusion

In this study, we have theoretically analysed the thermal rectification factor of a conductive thermal diode in a plane geometry, that is made of $VO_2$ and $SiO_2$ considering the Dirichlet boundary conditions under transient conditions. The heat flux density behaviour at the cold side of the thermal diode and its consequence on the thermal rectification factor of the thermal diode have been investigated deeply by considering various intrinsic and extrinsic parameters. It has been shown that the thermal conductivity and the specific heat capacity have a major impact on the nonlinear time behaviour of the thermal rectification under transient conditions. Furthermore, we obtained higher thermal rectification under transient conditions than steady-state conditions for almost all parameters values. There is an effect of the interface thermal resistance on the thermal rectification for both steady-state and transient conditions, but this effect seems to be minor generally in comparison with the other intrinsic parameters of the conductive thermal diode.

Considering the reasonable outcomes of this theoretical study, further research should be conducted on this type of conductive thermal diodes especially under different transient boundary conditions in order to demonstrate the full benefits of the transient analysis for a better control of practical thermal management systems. Pulsed and dynamical boundary conditions constitute a further step to understand and explore to get more insights onto the behaviour of the conductive thermal diode based on a phase change material and the phase change effects on the thermal rectification under these conditions.

## Acknowledgement

This article pertains to the France 2030 program “Investissements d’Avenir” (LABEX INTERACTIFS, reference ANR-11-LABX-0017-01). This article pertains to the French government program “Investissements d’Avenir” (EUR INTREE, reference ANR-18-EURE-0010).

## Declaration of competing interest

The authors declare that they have no known competing financial interests or personal relationships that could have appeared to influence the work reported in this paper.

## References

[1] Y. Li, W. Li, T. Han, X. Zheng, J. Li, B. Li, S. Fan, C.-W. Qiu, Transforming heat transfer with thermal metamaterials and devices, Nature Reviews Materials 6 (6) (2021) 488–507.

[2] M. Browne, B. Norton, S. McCormack, Phase change materials for photovoltaic thermal management, Renewable and Sustainable Energy Reviews 47 (2015) 762–782. doi:https://doi.org/10.1016/j.rser.2015.03.050.
URL https://www.sciencedirect.com/science/article/pii/S1364032115002038

[3] Z. Rao, S. Wang, A review of power battery thermal energy management, Renewable and Sustainable Energy Reviews 15 (9) (2011) 4554–4571. doi:https://doi.org/10.1016/j.rser.2011.07.096.
URL https://www.sciencedirect.com/science/article/pii/S1364032111003418

[4] A. Pasupathy, R. Velraj, R. Seeniraj, Phase change material-based building architecture for thermal management in residential and commercial establishments, Renewable and Sustainable Energy Reviews 12 (1) (2008) 39–64. doi:https://doi.org/10.1016/j.rser.2006.05.010.
URL https://www.sciencedirect.com/science/article/pii/S1364032106000724

[5] M. Wong, C. Tso, T. Ho, H. Lee, A review of state of the art thermal diodes and their potential applications, International Journal of Heat and Mass Transfer 164 (2021) 120607.

doi:https://doi.org/10.1016/j.ijheatmasstransfer.2020.120607.
URL https://www.sciencedirect.com/science/article/pii/S0017931020335432

[6] G. Wehmeyer, T. Yabuki, C. Monachon, J. Wu, C. Dames, Thermal diodes, regulators, and switches: Physical mechanisms and potential applications, Applied Physics Reviews 4 (4) (2017) 041304. arXiv:https://doi.org/10.1063/1.5001072, doi:10.1063/1.5001072.
URL https://doi.org/10.1063/1.5001072

[7] N. Roberts, D. Walker, A review of thermal rectification observations and models in solid materials, International Journal of Thermal Sciences 50 (5) (2011) 648–662. doi:https://doi.org/10.1016/j.ijthermalsci.2010.12.004.
URL https://www.sciencedirect.com/science/article/pii/S1290072910003443

[8] C. Starr, The copper oxide rectifier, Physics 7 (1) (1936) 15–19. arXiv:https://doi.org/10.1063/1.1745338, doi:10.1063/1.1745338.
URL https://doi.org/10.1063/1.1745338

[9] Z. Ding, Q.-X. Pei, J.-W. Jiang, W. Huang, Y.-W. Zhang, Interfacial thermal conductance in graphene/mos2 heterostructures, Carbon 96 (2016) 888–896. doi:https://doi.org/10.1016/j.carbon.2015.10.046.
URL https://www.sciencedirect.com/science/article/pii/S0008622315303560

[10] S. Li, Z.-X. Guo, J. Ding, Interface thermal transport of graphene-based intralayer heterostructures, Physica B: Condensed Matter 561 (2019) 164–169. doi:https://doi.org/10.1016/j.physb.2019.02.064.
URL https://www.sciencedirect.com/science/article/pii/S0921452619301590

[11] X.-K. Chen, Z.-X. Xie, Y. Zhang, Y.-X. Deng, T.-H. Zou,

J. Liu, K.-Q. Chen, Highly efficient thermal rectification in carbon/boron nitride heteronanotubes, Carbon 148 (2019) 532–539. doi:https://doi.org/10.1016/j.carbon.2019.03.073.
URL https://www.sciencedirect.com/science/article/pii/S0008622319302970

[12] H. Zhang, S. Xiong, H. Wang, S. Volz, Y. Ni, Thermal transport in graphene/h-bn lateral heterostructures with interface compositional diffusion, Europhysics Letters 125 (4) (2019) 46001. doi:10.1209/0295-5075/125/46001.
URL https://dx.doi.org/10.1209/0295-5075/125/46001

[13] T. Liang, M. Zhou, P. Zhang, P. Yuan, D. Yang, Multilayer in-plane graphene/hexagonal boron nitride heterostructures: Insights into the interfacial thermal transport properties, International Journal of Heat and Mass Transfer 151 (2020) 119395. doi:https://doi.org/10.1016/j.ijheatmasstransfer.2020.119395.
URL https://www.sciencedirect.com/science/article/pii/S0017931019350446

[14] D. B. Go, M. Sen, On the Condition for Thermal Rectification Using Bulk Materials, Journal of Heat Transfer 132 (12), 124502 (09 2010). arXiv:https://asmedigitalcollection.asme.org/heattransfer/article-pdf/132/12/124502/5794110/124502_1.pdf, doi:10.1115/1.4002286.
URL https://doi.org/10.1115/1.4002286

[15] A. Gupta, M. Talha, Recent development in modeling and analysis of functionally graded materials and structures, Progress in Aerospace Sciences 79 (2015) 1–14. doi:https://doi.org/10.1016/j.paerosci.2015.07.001.
URL https://www.sciencedirect.com/science/article/pii/S0376042115000561

[16] M. Naebe, K. Shirvanimoghaddam, Functionally graded materials: A

review of fabrication and properties, Applied Materials Today 5 (2016) 223–245. doi:https://doi.org/10.1016/j.apmt.2016.10.001.
URL https://www.sciencedirect.com/science/article/pii/S2352940716301214

[17] R. Dettori, C. Melis, R. Rurali, L. Colombo, Thermal rectification in silicon by a graded distribution of defects, Journal of Applied Physics 119 (21) (2016) 215102. arXiv:https://doi.org/10.1063/1.4953142, doi:10.1063/1.4953142.
URL https://doi.org/10.1063/1.4953142

[18] F. Yousefi, M. Shavikloo, M. Mohammadi, Non-equilibrium molecular dynamics study on radial thermal conductivity and thermal rectification of graphene, Molecular Simulation 45 (8) (2019) 646–651. arXiv:https://doi.org/10.1080/08927022.2019.1578354, doi:10.1080/08927022.2019.1578354.
URL https://doi.org/10.1080/08927022.2019.1578354

[19] S. Raoux, Phase change materials, Annual Review of Materials Research 39 (1) (2009) 25–48. arXiv:https://doi.org/10.1146/annurev-matsci-082908-145405, doi:10.1146/annurev-matsci-082908-145405.
URL https://doi.org/10.1146/annurev-matsci-082908-145405

[20] F. J. Morin, Oxides which show a metal-to-insulator transition at the neel temperature, Phys. Rev. Lett. 3 (1959) 34–36. doi:10.1103/PhysRevLett.3.34.
URL https://link.aps.org/doi/10.1103/PhysRevLett.3.34

[21] G. Andersson, C. Parck, U. Ulfvarson, E. Stenhagen, B. Thorell, Studies on vanadium oxides. ii. the crystal structure of vanadium dioxide., Acta Chemica Scandinavica 10 (1956) 623–628.

[22] D.-W. Oh, C. Ko, S. Ramanathan, D. G. Cahill, Thermal conductivity and dynamic heat capacity across the metal-insulator transition in thin

film vo2, Applied Physics Letters 96 (15) (2010) 151906. arXiv:https://doi.org/10.1063/1.3394016, doi:10.1063/1.3394016.
URL https://doi.org/10.1063/1.3394016

[23] Y. Yang, H. Chen, H. Wang, N. Li, L. Zhang, Optimal thermal rectification of heterojunctions under fourier law, Phys. Rev. E 98 (2018) 042131. doi:10.1103/PhysRevE.98.042131.
URL https://link.aps.org/doi/10.1103/PhysRevE.98.042131

[24] S. O. Kasali, J. Ordonez-Miranda, K. Joulain, Conductive thermal diode based on two phase-change materials, International Journal of Thermal Sciences 153 (2020) 106393. doi:https://doi.org/10.1016/j.ijthermalsci.2020.106393.
URL https://www.sciencedirect.com/science/article/pii/S1290072919317752

[25] H. Kang, F. Yang, J. J. Urban, Thermal rectification via heterojunctions of solid-state phase-change materials, Phys. Rev. Applied 10 (2018) 024034. doi:10.1103/PhysRevApplied.10.024034.
URL https://link.aps.org/doi/10.1103/PhysRevApplied.10.024034

[26] A. L. Cottrill, S. Wang, A. T. Liu, W.-J. Wang, M. S. Strano, Dual phase change thermal diodes for enhanced rectification ratios: Theory and experiment, Advanced Energy Materials 8 (11) (2018) 1702692. arXiv:https://onlinelibrary.wiley.com/doi/pdf/10.1002/aenm.201702692, doi:https://doi.org/10.1002/aenm.201702692.
URL https://onlinelibrary.wiley.com/doi/abs/10.1002/aenm.201702692

[27] J. Ordonez-Miranda, J. M. Hill, K. Joulain, Y. Ezzahri, J. Drevillon, Conductive thermal diode based on the thermal hysteresis of vo2 and nitinol, Journal of Applied Physics 123 (8) (2018) 085102. arXiv:https://doi.org/10.1063/1.5019854, doi:10.1063/1.5019854.
URL https://doi.org/10.1063/1.5019854

[28] S. O. Kasali, J. Ordonez-Miranda, K. Alaili, K. Joulain, Spherical and cylindrical conductive thermal diodes based on two phase-change materials, Zeitschrift für Naturforschung A 77 (2) (2022) 181–190 [cited 2022-12-06]. doi:doi:10.1515/zna-2021-0170.
URL https://doi.org/10.1515/zna-2021-0170

[29] F. A. Herrera, T. Luo, D. B. Go, Thermal Rectification Under Transient Conditions: The Role of Thermal Capacitance and Thermal Conductivity, Journal of Heat Transfer 139 (9), 091301 (05 2017). arXiv:https://asmedigitalcollection.asme.org/heattransfer/article-pdf/139/9/091301/6215395/ht_139_09_091301.pdf, doi:10.1115/1.4036339.
URL https://doi.org/10.1115/1.4036339

[30] K. Klinar, M. Muñoz Rojo, Z. Kutnjak, A. Kitanovski, Toward a solid-state thermal diode for room-temperature magnetocaloric energy conversion, Journal of Applied Physics 127 (23) (2020) 234101. arXiv:https://doi.org/10.1063/5.0006120, doi:10.1063/5.0006120.
URL https://doi.org/10.1063/5.0006120

[31] J. Ordonez-Miranda, Y. Ezzahri, K. Joulain, J. Drevillon, J. J. Alvarado-Gil, Modeling of the electrical conductivity, thermal conductivity, and specific heat capacity of $vo_2$, Phys. Rev. B 98 (2018) 075144. doi:10.1103/PhysRevB.98.075144.
URL https://link.aps.org/doi/10.1103/PhysRevB.98.075144

[32] C. N. Berglund, H. J. Guggenheim, Electronic properties of $vo_2$ near the semiconductor-metal transition, Phys. Rev. 185 (1969) 1022–1033. doi:10.1103/PhysRev.185.1022.
URL https://link.aps.org/doi/10.1103/PhysRev.185.1022

[33] W. bin Yuan, N. Yu, L. yuan Li, Y. Fang, Heat transfer analysis in multi-layered materials with interfacial thermal resistance, Composite Structures 293 (2022) 115728. doi:https:

//doi.org/10.1016/j.compstruct.2022.115728.
URL https://www.sciencedirect.com/science/article/pii/S0263822322005050